Biosensors and Bioelectronics 87 (2017) 473–479

Contents lists available at ScienceDirect

Biosensors and Bioelectronics

journal homepage: www.elsevier.com/locate/bios

Hollow TiO_2 modified reduced graphene oxide microspheres encapsulating hemoglobin for a mediator-free biosensor

Hui Liu*, Kai Guo, Congyue Duan, Xiaonan Dong, Jiaojiao Gao

School of Materials Science and Engineering, Shaanxi University of Science and Technology, Xi'an 710021, PR China

ARTICLE INFO

Article history:
Received 22 July 2016
Received in revised form
25 August 2016
Accepted 26 August 2016
Available online 30 August 2016

Keywords:
Graphene
Hollow microsphere
Direct electrochemistry
Biosensor
Long-term stability

ABSTRACT

Hollow TiO_2 modified reduced graphene oxide microspheres (hollow TiO_2-rGO microspheres or H-TiO_2-rGO MS) have been synthesized and then be used to immobilize hemoglobin (Hb) to fabricate a mediator-free biosensor. The morphology and structure of hollow TiO_2-rGO microspheres were characterized by scanning electron microscopy, transmission electronic microscopy and X-ray diffraction. Results of spectroscopy and electrochemistry tests revealed that hollow TiO_2-rGO microsphere is an excellent immobilization matrix with biocompatibility for redox protein, affording good protein bioactivity and stability. The hollow TiO_2-rGO microspheres with special structure and component enhance the immobilization efficiency of proteins and facilitate the direct electron transfer, which result in the better H_2O_2 detection performance-the wide linear range of 0.1–360 μM for H_2O_2 (sensitivity of 417.6 μA mM^{-1} cm^{-2}) and the extremely low detection limit of 10 nM for H_2O_2. Moreover, the hollow microsphere can provide a protective microenvironment for Hb to make the as-prepared biosensor improve long-term stability. The as-prepared biosensor retains 95.4% of the initial response to H_2O_2 after 60-d storage. Hence, this work suggests that if can be fabricated a mediator-free biosensor, hollow TiO_2-rGO microspheres will find wide potential applications in environmental analysis and biomedical detection.

1. Introduction

Graphene, an atomic sheet of sp^2 bonded carbon atoms, possesses a high specific surface area (~2600 m^2 g^{-1}), extraordinary electronic transport properties (20,000 cm^2 V^{-1} s^{-1}) and high electrocatalytic activities (Akhavan and Ghaderi, 2009; Allen Mattew et al., 2010; Park et al., 2008; Park and Ruoff 2009). Furthermore, graphene with the unique two-dimensional crystal structure can anchor or wrap metal and metal oxide nanoparticles effectively to form many kinds of nanocomposites, offering versatile selective catalytic or sensing performances (Dong et al., 2010; Lee et al., 2012; Liu et al., 2012; Shan et al., 2010; Zhang et al., 2010). TiO_2-graphene nanocomposites have drawn great attention among many kinds of nanocomposites because TiO_2 owns superior photocatalytic performance, good biocompatibility, pollution-free environment and chemical and thermal stabilities (Fan et al., 2011; Liu et al., 2013; Liu and Chen, 2005; Sun et al., 2013; Wang et al., 2015). Recent studies demonstrated that TiO_2-graphene nanocomposite is a promising electrode material for electrochemical sensing applications (Cao et al., 2013; Jang et al., 2012; Liu et al., 2014a). In these biosensors, TiO_2-graphene, facilitating the direct electron transfer and enhancing the catalytic activity of enzymes, was always employed as a matrix for immobilizing enzymes. Meanwhile, Kim and coworkers reported that the immobilization quality of enzyme, which determines the property of biosensor, is influenced by the morphology and structure of nanocomposites (Kim et al., 2006; Xie et al., 2011). Although substantial effort has been devoted to the development of new nanostructured materials for use in biosensors, achieving new morphologies of TiO_2-graphene nanocomposites with high performance is still a challenge (Xie et al., 2011).

In this paper, the hollow TiO_2 modified reduced graphene oxide microspheres (hollow TiO_2-rGO microspheres or H-TiO_2-rGO MS) were synthesized successfully. The bag-like structure make hollow microsphere with a breach as a matrix of enzymes has many advantages as follows. Firstly, as shown in Fig. 1, the inner space of the "bag" allows more quantity of enzymes to be immobilized. Meanwhile, some enzyme can be absorbed on outside of the hollow rGO sphere. Secondly, TiO_2 nanoparticles with excellent biocompatibility can provide a protective microenvironment for the enzymes to retain their enzymatic stability and activity and the nanoscaled TiO_2 particles (less than 10 nm in diameter) can greatly enhance the active surface area which is available for adsorbing protein. Thirdly, the substrate can easily be entrapped by graphene with a high surface area. Some of the absorbed substrate has the chance to pass the defects on rGO to get into the hollow

* Corresponding author.
E-mail address: liuhui@sust.edu.cn (H. Liu).

http://dx.doi.org/10.1016/j.bios.2016.08.089
0956-5663/

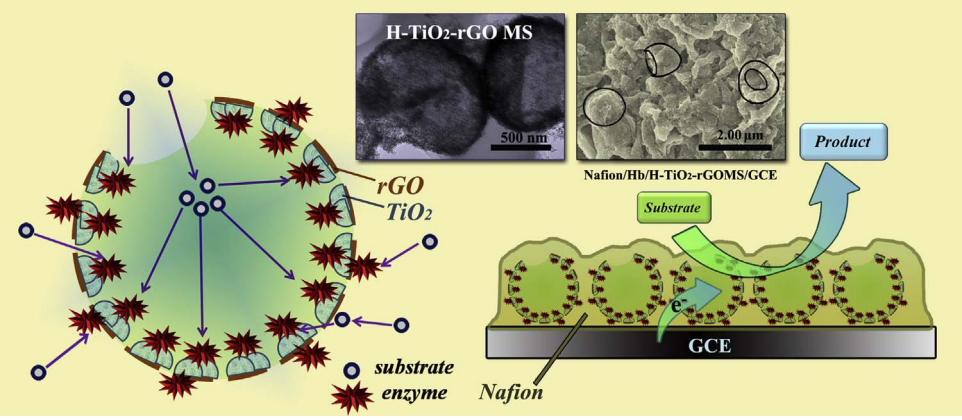

Fig. 1. Schematic illustration of the hollow TiO_2-rGO microsphere encapsulating hemoglobin and Nafion/Hb/TiO_2-rGO MS/GCE.

sphere resulting in substrate's enrichment. The rGO is converted from GO by hydrothermal method and rGO's two dimensional crystal structure has lots of defects. Concentration of substrate and enzyme in this confined region will increase the chance of effective collisions between them (Xie et al., 2011). Finally, graphene, for its excellent mobility of charge carriers, is able to become an excellent media to promote electrical communication between enzyme and electrode. Thus, hollow TiO_2-rGO microsphere is a promising support for enzyme immobilization and has potential applications in biosensors.

In this work, hemoglobin (Hb) was selected as a model redox protein to construct a biosensor. The performance of a sensor composed of Hb immobilized in the hollow TiO_2-rGO microspheres was compared with that of sensors based on TiO_2, rGO, solid TiO_2@rGO microspheres and sheet TiO_2-rGO nanocomposite in order to highlight the advantages of the hollow TiO_2-rGO microsphere as a support.

2. Experimental

2.1. Materials and apparatus

Hb (from bovine blood) and Nafion solution (5 wt% in lower aliphatic alcohols) are purchased from Sigma. Unless otherwise noted, all other chemicals (analytical grade) are purchased from Sinopharm Chemical Reagent Co., Ltd., China. In all experiments, deionized water is used.

Field-emission scanning electron microscopy (FE-SEM) is performed using a Hitachi S-4800 & Hiroba energy dispersive X-ray electron microscopy. Transmission electronic microscopy (TEM) images are obtained on a Hitachi H-800 instrument. X-ray diffraction (XRD) patterns are recorded on a Rigaku D/max 2200 pc diffractometer using Cu Kα radiation of wavelength $\lambda = 0.15418$ nm at 40 kV and 40 mA. Raman spectra are taken using an ALPHA 300 M Micro-Raman spectrometer system. UV–vis spectra are recorded using a PerkinElmer Lambda-950 spectrophotometer. All electrochemical experiments are performed with a CHI 660D electrochemical workstation (CH Instruments, Shanghai, China). A conventional three-electrode system which consists of a platinum wire as the counter electrode, an Ag/AgCl/3 M KCl as the reference electrode and a 3-mm diameter modified glassy carbon electrode (GCE) as the working electrode is used in all electrochemical experiments. Unless otherwise noted, 0.1 M phosphate buffered saline (PBS; pH 7.0) is used as the supporting electrolyte in all experiments. The buffer is purged with highly purified nitrogen for at least 30 min and a nitrogen atmosphere environment is kept in electrochemical measurements.

2.2. Preparation of hollow TiO_2-rGO microspheres

Graphene oxide (GO) was prepared from graphite powder by the modified Hummers method (Hummers Jr and Offeman, 1958; Kovtyukhova et al., 1999), while TiO_2 precursor microspheres and TiO_2@GO microspheres were prepared by the method in our previous references (Liu et al., 2013). The typical preparation steps of hollow TiO_2-rGO microspheres are shown in Fig. 2A. The preparation of hollow TiO_2-rGO microspheres adopts HCl etching reaction under the hydrothermal condition. In this preparation, the 1 g TiO_2@GO microspheres were dispersed in 70 mL mixture of ethanol and HCl solution ($V_{[ethanol]}$: $V_{[HCl]} = 1:1$) by high-speed stirring. After a high-speed stirring about 15 min, the suspension was loaded in a 100 mL Teflon-lined autoclave. The autoclave was sealed and then heated in an oven of 180 °C for 24 h. As a result, black flocculent products (hollow TiO_2-rGO microspheres) were formed. Next, the flocculent products were collected, washed with ethanol and distilled water for several times to remove ions and possible remnants and dried at 50 °C. For comparison, solid TiO_2@rGO microspheres (TiO_2@rGO MS) were synthesized by the similar procedure without HCl solution (Fig. S1). Meanwhile, sheet TiO_2-rGO nanocomposite was prepared by the method in our previous references (Fig. S2) (Liu et al., 2014b).

2.3. Preparation of enzyme electrode

To investigate the electrochemical behavior of H-TiO_2-rGO MS based biosensor, enzyme electrode is assembled. Prior to use, the GCE was sequentially polished using 1.0, 0.3 and 0.05 μm alumina powder on a polishing cloth and rinsing with deionised water. The electrode is then sonicated in ethanol and deionised water. Next, the electrode is dried using a purified nitrogen stream. The enzyme electrode was prepared by a simple casting method. Firstly, 1 mL of 2 mg mL^{-1} H-TiO_2-rGO MS suspension and 0.5 mL of 10 mg mL^{-1} Hb PBS are mixed and then stirred for 20 min. Next, 0.5 mL of Nafion (5%) was added to the mixture and then stirred for 10 min. A suspension (denoted as Suspension I) finally contains a concentration of 2.5 mg mL^{-1} Hb, 1 mg mL^{-1} H-TiO_2-rGO MS and 1.25% Nafion. Finally, 4 μL of Suspension I is dropped to the surface of a freshly polished GCE to prepare the Nafion/Hb/H-TiO_2-rGOMS/GCE. A beaker is covered over the electrode so that water can evaporate slowly in air and a uniform film electrode can be obtained. The dried Nafion/Hb/H-TiO_2-rGOMS/ GCE are stored at 4 °C in refrigerator when the electrode is not use.

For comparison, TiO_2, rGO, solid TiO_2@rGO MS and sheet TiO_2-rGO are used for the fabrication of Nafion/Hb/TiO_2/GCE, Nafion/Hb/rGO/GCE, Nafion/Hb/TiO_2@rGOMS/GCE and Nafion/Hb/TiO_2-rGO/GCE through similar procedures as described above. In the

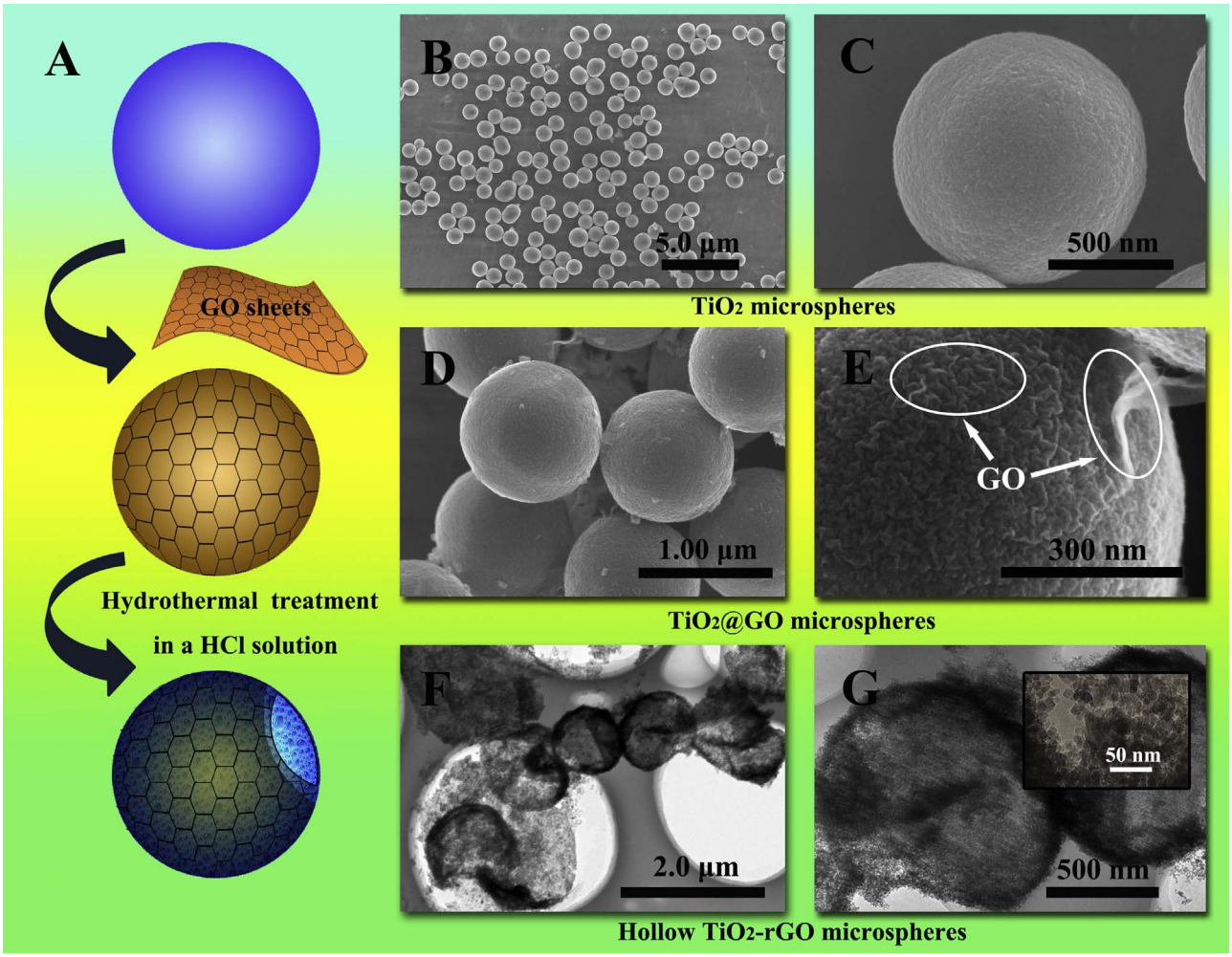

Fig. 2. Schematic illustration of synthesis steps for hollow TiO_2-rGO microspheres and corresponding SEM or TEM images. (A) Synthesis steps for hollow TiO_2-rGO microspheres. (B and C) SEM images of bare TiO_2 microspheres. (D and E) SEM images of TiO_2@GO microspheres. (F and G) TEM images of as-prepared hollow TiO_2-rGO microsphere.

control experiment, Nafion/Hb/GCE and Nafion/H-TiO_2-rGOMS/GCE are also prepared. Before electrochemical measurements, all the as-prepared film electrodes are immersed in pH 7.0 PBS for 30 min to remove residual components.

3. Results and discussions

3.1. Characterization of hollow TiO_2-rGO microspheres

Fig. 2 displays schematic illustration of synthesis steps of hollow TiO_2-rGO microspheres and corresponding typical SEM or TEM images of the samples prepared at various stages. As shown in Fig. 2A, the synthesis steps are mainly as follows: firstly, TiO_2 microspheres were synthesized by a controlled hydrolysis of tetrabutyl titanate in ethanol. Secondly, the TiO_2 microspheres were directly wrapped by graphene oxide (GO) nanosheets to form TiO_2@GO (Liu et al., 2013). Finally, the hollow TiO_2-rGO microspheres were synthesized by HCl etching reaction under the hydrothermal condition. From Fig. 2B and C, it is observed that TiO_2 microspheres show relatively uniform morphology with diameters about 1 μm and the TiO_2 microspheres own smooth surface (Fig. 2C). Fig. 2D and E presents that the spherical morphology of TiO_2@GO microspheres were not changed after the wrapped process. It's worth noting that different from that of the pure TiO_2 microspheres, the surface of the TiO_2@GO microspheres presents a wrinkle-like morphology, which indicates that the surface of TiO_2 microsphere was wrapped by GO nanosheets (Fig. 2E). From Fig. 2F and G, the hollow microspheres have been formed after hydrothermal treatment in HCl solution resulting from its etching reaction to TiO_2. However, graphene sheets remain lots of TiO_2 nanoparticles because etching reaction cannot fully remove TiO_2. Interestingly, almost every hollow microsphere has a breach, which can act as a channel for material to migrate outside, in other word, the hollow microsphere with a breach can form a bag-like structure, which is very benefit for enzyme's encapsulation. Meanwhile, nanoscaled TiO_2 particles not only have plentiful active surface area available to adsorb enzyme, but also have good biocompatibility to offer protective microenvironment for enzyme to keep its bioactivity. Hence, the hollow TiO_2-rGO microsphere is an excellent matrix for immobilizing enzyme.

Fig. S3 presents XRD patterns of GO (curve a), rGO (curve b), H-TiO_2-rGO MS (curve c) and TiO_2 (curve d) respectively. It can be seen that the XRD pattern of GO (curve a) shows a major peak at $2\theta = 10.5°$, corresponding to a D-spacing of 0.841 nm, which is much larger than the d-spacing of natural graphite at 0.335 nm. This change indicates that graphite is oxidized to form GO (Sher Shah et al., 2012). After hydrothermal treatment, this peak disappears and a new peak appears centered at $2\theta = 24.2°$, corresponding to the 0.367 nm d-spacing of graphene (curve b), indicating the reduction of GO to rGO (Bai et al., 2009). Curve c in Fig. S3 exhibits the XRD pattern of the as-prepared H-TiO_2-rGO

MS, all the diffraction peaks are good agreement with that of anatase TiO_2 (curve d). However, the diffraction peaks of rGO belong to H-TiO_2-rGO MS are not distinguishable in XRD patterns. This phenomenon can be ascribed to the much lower crystalline extent of rGO than that of TiO_2, which leads to the shielding of the rGO peaks by those of TiO_2 (Fan et al., 2011; Sher Shah et al., 2012; Zhang et al., 2009).

Fig. S4 presents Raman spectra of GO (curve a), rGO (curve b), TiO_2 (curve c) and H-TiO_2-rGO MS (curve d) respectively. All of GO, rGO and H-TiO_2-rGO MS show the same Raman shift at 1355 and 1598 cm^{-1} corresponding to the D- and G-bands of graphene respectively. However, it can be found that the D/G intensity ratio increases from 0.99 (GO) to 1.10 (H-TiO_2-rGO MS or rGO) after the hydrothermal treatment, which can be attributed to the increase in the number of smaller sp^2 domains and a re-establishment of conjugated graphene networks (rearomatization) (Stankovich et al., 2007), suggesting a successful transformation of GO to rGO (Kudin et al., 2008; Xiang et al., 2012). Meanwhile, the increase of D-bond intensity demonstrates the increase of graphene's defects (Pham et al., 2011). These defects, the accesses of substrate to enter the inner hollow sphere, are benefit for enzymatic reaction. The Raman spectra of TiO_2 (curve c) shows the presence of peaks at 158, 408, 513 and 630 cm^{-1} can be attributed to the $E_{g(1)}$, $B_{1g(1)}$, $A_{1g}+B_{1g(2)}$, and $E_{g(2)}$ modes of anatase phase of TiO_2 (Xiang et al., 2012; Yu et al., 2011). Curve d show all the Raman bands for anatase phase of TiO_2 and rGO, confirms the co-existence of anatase TiO_2 and rGO in the nanocomposite.

3.2. Encapsulation of Hb in the Nafion/Hb/H-TiO_2-rGO MS composite film

Fig. S5A exhibits a typical TEM image of Hb/H-TiO_2-rGO MS. Due to the high surface area and the bag-like structure of the hollow microsphere, H-TiO_2-rGO MS loads a lot of Hb. Fig. S5B depicts the microstructure image of Nafion/Hb/H-TiO_2-rGOMS composite film. It is noted that the hollow microsphere with a bag-like structure is discernible on the surface of modified electrode. H-TiO_2-rGO MS was embedded in the Nafion to form a stable composite film, which was essential for the stability of the prepared enzyme electrode. Moreover, because of the high surface area of H-TiO_2-rGO MS, the effective surface area of the modified electrode improves greatly.

The stability of Hb immobilized both in H-TiO_2-rGO MS and Nafion/Hb/H-TiO_2-rGOMS composite film was investigated by UV–vis spectroscopy (Sun et al., 2014a; Wang et al., 2015). The Soret absorption bands of heme proteins provide information about the conformational integrity of the proteins. As shown in Fig. S5C, the Soret absorption band of Hb immobilized in H-TiO_2-rGO MS (curve a) and Nafion/Hb/H-TiO_2-rGOMS composite film (curve b) is located at about 405 nm which is close to that of native Hb at 406 nm (curve c), indicating the Hb retained the essential features of its conformational integrity, also revealing that hollow TiO_2-rGO microspheres have biocompatibility and did not suffer significant protein denaturation.

3.3. Electrochemical characteristics of the modified electrodes

Fig. 3 shows the typical cyclic voltammograms (CVs) of different modified electrodes in 0.1 M PBS (pH 7.0) at a scan rate of 0.1 V s^{-1}. No redox peak is observed at Nafion/H-TiO_2-rGOMS/GCE (curve a), which indicates that Nafion/H-TiO_2-rGOMS/GCE is electroinactive in the given potential window. The Nafion/Hb/H-TiO_2-rGOMS/GCE (curve g) exhibits a couple of stable and well-defined redox peaks at −0.369 V and −0.334 V vs. Ag/AgCl, which can be ascribed to direct electron transfer (DET) between Hb and the underlying electrode (Sun et al., 2013). The formal potential

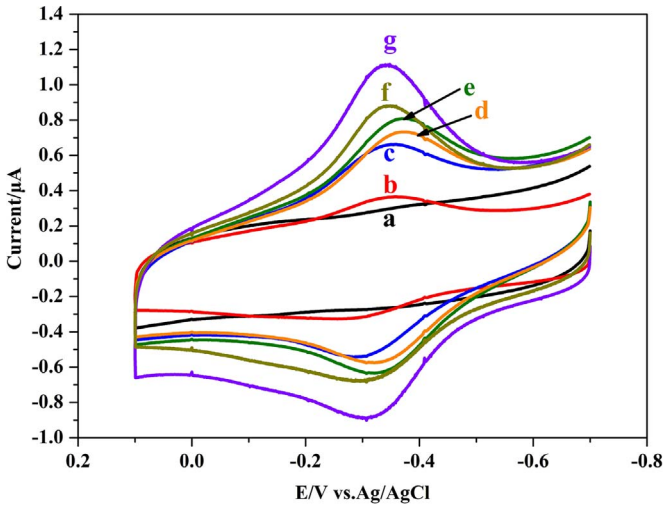

Fig. 3. Cyclic voltammograms of Nafion/H-TiO_2-rGOMS/GCE (curve a), Nafion/Hb/GCE (curve b), Nafion/Hb/TiO_2/GCE (curve c), Nafion/Hb/rGO/GCE (curve d), Nafion/Hb/TiO_2-rGO/GCE (curve e), Nafion/Hb/TiO_2@rGOMS/GCE (curve f), Nafion/Hb/H-TiO_2-rGOMS/GCE (curve g) in 0.1 M pH 7.0 PBS with a scan rate of 0.1 V s^{-1}.

($E^{0'}=(E_{p,a}+E_{p,c})/2$) of Hb is −0.351 V vs. Ag/AgCl, in agreement with −0.345 V and −0.353 V vs. Ag/AgCl reported for the Hb($Fe^{III/II}$) redox couple in Hb-ZnO-MWCNTs-Nafion (Ma and Tian, 2010) and Hb-TiO_2-MXene-Nafion (Wang et al., 2015) films. Compared with that of the Nafion/Hb/H-TiO_2-rGOMS/GCE, the redox peaks observed at the Nafion/Hb/GCE (curve c, in Fig. 3) are 87.3% smaller, suggesting an enhanced electron transfer between Hb molecules and the surface of the Nafion/Hb/H-TiO_2-rGOMS/GCE. Meanwhile, the much smaller redox peaks of Nafion/Hb/GCE can be attributed to the denaturation of proteins on the bare electrode surface and the difficulty for proteins realizing the DET process on the bare electrode (Dong et al., 2011a; Wang et al., 2015; Zhu et al., 2011). It can be clearly seen from Fig. 3 that direct electron transfer between Hb molecules and GCE is greatly enhanced at the Nafion/Hb/H-TiO_2-rGOMS/GCE. For comparison, Nafion/Hb/TiO_2/GCE (curve c), Nafion/Hb/rGO/GCE (curve d), Nafion/Hb/TiO_2-rGO/GCE (curve e) and Nafion/Hb/TiO_2@rGO MS/GCE (curve f) have also been carried out. The redox peaks of these four electrodes are smaller than that of Nafion/Hb/H-TiO_2-rGOMS/GCE. It can conclude that hollow TiO_2-rGO microspheres have better effect on the facilitation of electron transfer, which may resulted from their unique morphology and structure.

Fig. S6 shows the cyclic voltammograms of Nafion/Hb/H-TiO_2-rGOMS/GCE at 0.1 M PBS (pH 7.0) with the scan rate increasing from 0.1 to 0.8 V s^{-1}. With the increase of the scan rate, the cathodic and anodic peak currents of Hb increase simultaneously and the cathodic and anodic peak potentials show a small shift resulting in the peak to peak separation slightly enlarged. The inset of Fig. S6 shows that the cathodic (i_{pc}) and anodic (i_{pa}) peak currents increase linearly with scan rates increased from 0.1 to 0.8 V s^{-1}. It reveals that the electrode reaction corresponds to a surface attached reaction process. Moreover, the slopes of anodic and cathodic processes are nearly equal, suggesting that Hb is stable and not undergoing denaturation. Using the Laviron method for a surface-controlled electrochemical system (Laviron, 1979), the apparent heterogeneous electron transfer rate constant (k_s) of Hb immobilized on Nafion/Hb/H-TiO_2-rGOMS/GCE is estimated about 3.27 s^{-1}, which is higher than the value reported for Hb immobilized TiO_2 nanorods-graphene (0.65 s^{-1}) (Sun et al., 2013) and nitrogen-doped graphene (2.36 s^{-1}) (Sun et al., 2014b), suggesting a faster electron-transfer process. This means that hollow TiO_2-rGO microspheres facilitates the direct electron transfer of Hb.

The average surface concentration of electroactive Hb (Γ^*, mol cm^{-2}) can be estimated from the charge integration of the reduction peak of the CV using the formula:

$$Q = nFA\Gamma^* \quad (1)$$

where F is Faraday constant, Q is the charge (C) and can be obtained by integrating the reduction peak of Hb, n and A stand for the number of electron transferred and the geometrical surface area of the electrode, respectively. According to this method, the surface concentration of electroactive Hb (Γ^*) *at* Nafion/Hb/H-TiO_2-rGOMS/GCE was calculated as 5.26×10^{-10} mol cm^{-2}, which is much greater than the theoretical value for monolayer coverage (1.89×10^{-11} mol cm^{-2}) (Wang et al., 2005). This means that multilayer of Hb entrapped in the Nafion/Hb/H-TiO_2-rGOMS composite film participates in the electron-transfer process. Meanwhile, the surface concentration of electroactive Hb of Nafion/Hb/H-TiO_2-rGOMS/GCE is higher than that of Nafion/Hb/TiO_2@rGOMS/GCE (4.30×10^{-10} mol cm^{-2}) and Nafion/Hb/TiO_2-rGO/GCE (3.82×10^{-10} mol $cm_)^{-2}$, revealing that hollow TiO_2-rGO microspheres can immobilize more Hb and retain its activity and stability on the surface of GCE.

Fig. S7 shows that the cyclic voltammograms of Nafion/Hb/H-TiO_2-rGOMS/GCE in different pH values 0.1 M PBS. Stable and well-defined CVs are observed in the pH values range 6.0–8.0. With the increase of pH value, both the cathodic and anodic peaks shifted to the negative. This can be contributed to the involvement of proton transfer in the Hb(Fe^{III})/Hb(Fe^{II}) redox couple (Chen et al., 2015). The $E^{0'}$ value of Hb varied linearly in the range of pH values of 6.0–8.0, with a slop of -54.2 mV pH^{-1} (the inset of Fig. S7). This value is very close to the theoretical value for the transfer of one proton and electron in a reversible reduction (-58 mV pH^{-1} at 25 °C) (Chen et al., 2015; Xie et al., 2011).

3.4. Electrocatalytic properties of the Nafion/Hb/H-TiO_2-rGOMS/GCE

Hb usually exhibits electrocatalytic activity for H_2O_2, nitrite and Cl_3CCOOH after Hb with retained bioactivity is immobilized on an electrode surface (Dong et al., 2011a; Lu et al., 2008; Sun et al., 2013). Using H_2O_2 as a probe, we investigated the electrocatalytic properties of the Nafion/Hb/H-TiO_2-rGOMS/GCE. As shown in Fig. 4, the reduction peak increases dramatically with the increasing of H_2O_2 concentration and the oxidation peak decreases and disappears display the obvious electrocatalytic behavior of Hb for the reduction of H_2O_2. A possible reaction mechanism of H_2O_2 catalyzed by the Hb-based electrode is postulated as follows (George and Lee, 2009):

$$\mathrm{Hb}\left(Fe^{III}\right) + e^- \rightleftharpoons \mathrm{Hb}\left(Fe^{II}\right) \quad (2)$$

$$\mathrm{Hb}\left(Fe^{II}\right) + H_2O_2 + 2H^+ \rightarrow \mathrm{Hb}\left(Fe^{III}\right) + 2H_2O \quad (3)$$

With the increasing of H_2O_2 concentration, the current value tents to saturation limit (the inset of Fig. 4) and the saturation behavior is characteristic of enzyme-based catalysis. The apparent Michaelis-Menten constant (K_M^{app}) can be obtained by the electrochemical-version of Lineweaver-Burk equation (Kamin and Wilson, 1980):

$$\frac{1}{I_{ss}} = \frac{K_M^{app}}{I_{max}C} + \frac{1}{I_{max}} \quad (4)$$

where I_{ss} is the steady-state current after the addition of substrate, C is the bulk concentration of the substrate, and I_{max} is the maximum current measured under saturated substrate conditions. The K_M^{app} value of Nafion/Hb/H-TiO_2-rGOMS/GCE is estimated to be 141.4 μM (curve a in Fig. S8). This value is smaller than those ever reported values of 180 μM (Dong et al., 2011b) and 379 μM (Sun et al., 2012), indicating that Hb immobilized on Nafion/Hb/H-TiO_2-rGOMS/GCE retained higher bioactivity and had a high biological affinity to H_2O_2. Note that the K_M^{app} value of Nafion/Hb/H-TiO_2-rGOMS/GCE is also smaller than that of Nafion/Hb/TiO_2@rGOMS/GC (184.9 μM) and Nafion/Hb/TiO_2-rGO/GCE (198.2 μM) (curve b and c in Fig. S8, respectively), which reveals that this hollow structure is more favorable to make immobilized Hb keep bioactive.

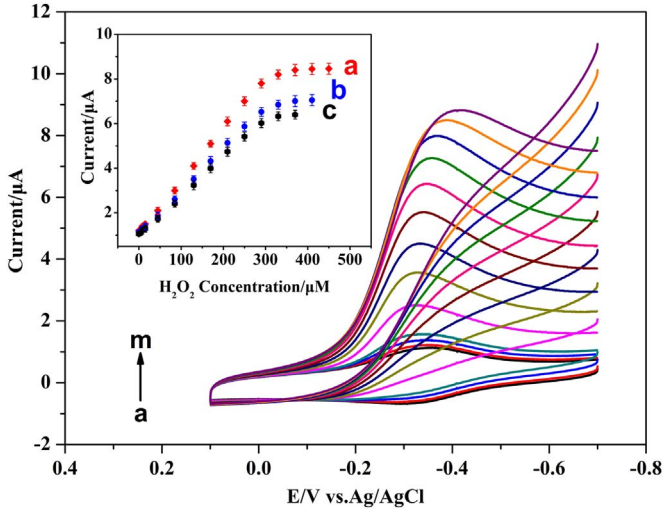

Fig. 4. Cyclic voltammograms of Nafion/Hb/H-TiO_2-rGOMS/GCE in 0.1 M pH 7.0 PBS containing 0 (a), 5 (b), 15 (c), 30 (d), 70 (e), 110 (f), 150 (g), 190 (h), 230 (i), 270 (j), 310 (k), 350 (l), 390 (m) H_2O_2 with a scan rate of 0.1 V s^{-1}. Inset: plot of the cathodic peak current vs H_2O_2 concentration: Nafion/Hb/H-TiO_2-rGOMS/GCE (curve a), Nafion/Hb/TiO_2@rGOMS/GCE (curve b), Nafion/Hb/TiO_2-rGO/GCE (curve c).

3.5. Biosensor performance of the Nafion/Hb/H-TiO_2-rGOMS/GCE

The biosensor performance for the detection of H_2O_2 of the Nafion/Hb/H-TiO_2-rGOMS/GCE was also investigated through amperometry method. Fig. 5 gives the amperometric responses of the modified glassy carbon electrodes at -0.35 V as adding H_2O_2 in stirred PBS (pH 7.0). Fig. 5A demonstrates that, on Nafion/Hb/H-TiO_2-rGOMS/GCE, the response time (achieving 95% of the steady-state current) is less than 3 s. And Fig. 5B indicates that, for Nafion/Hb/H-TiO_2-rGOMS/GCE, a well-defined linear relationship between the current and the H_2O_2 concentration is observed. The calibration plot shows a linear range from 0.1 to 360 μM (correlation coefficient of 0.999, N=24) with a sensitivity of 417.6 μA mM^{-1} cm^{-2} and a detection limit of 10 nM (based on a signal-to-noise ratio of 3).

Performances of various H_2O_2 biosensors are listed in Table S1. It is clear that the performance of Nafion/Hb/H-TiO_2-rGOMS/GCE is significantly improved. Furthermore, as can be seen from Fig. S9 and Table S2, compared with Nafion/Hb/TiO_2-rGO/GCE and Nafion/Hb/TiO_2@rGOMS/GCE, the H-TiO_2-rGO MS based biosensor has better performance. There are some reasons why the Nafion/Hb/H-TiO_2-rGOMS/GCE displays both a lower detection limit and a wider linear range. Firstly, the microsphere's hollow structure allows a lot of enzymes to be immobilized. Secondly, TiO_2 nanoparticles with excellent biocompatibility can provide a protective microenvironment for the enzymes to retain their enzymatic stability and activity. Essentially, the substrate can easily be entrapped by graphene with a high surface area and enter the inner space of microspheres through the quantities of rGO defects resulting in substrate's enrichment. Concentration of substrate and enzyme in this confined region will increase the chance of effective collisions

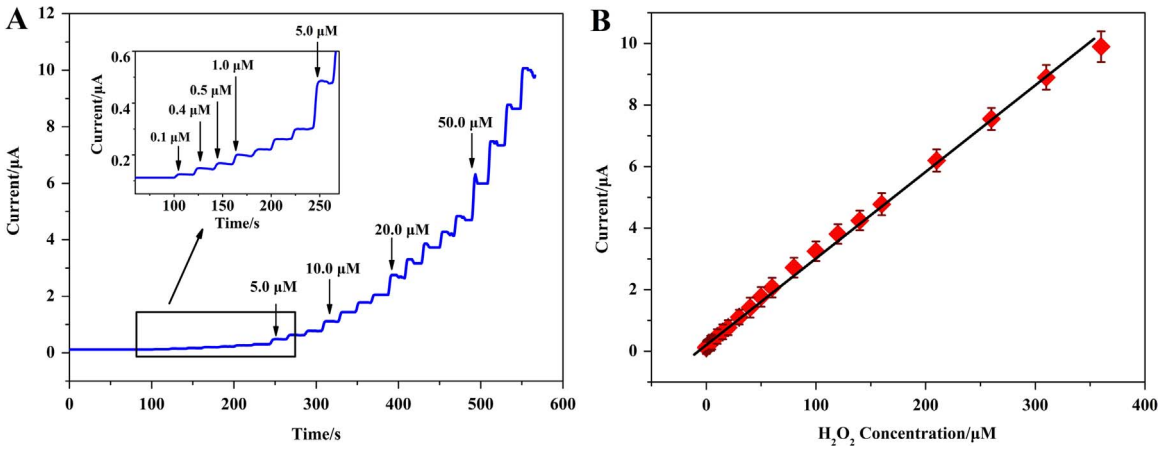

Fig. 5. (A) Typical current-time response of Nafion/Hb/H-TiO_2-rGOMS/GCE at −0.35 V to successive addition of H_2O_2 in stirred 0.1 M pH 7.0 PBS. (B) The steady state current vs · H_2O_2 concentration.

between them (Xie et al., 2011).

3.6. Selectivity of the H_2O_2 biosensor

Selectivity is important in practical use of the biosensors. The selectivity of the biosensor is evaluated by using the amperometric current-time method among nine typical interfering substances (ascorbic acid (b), dopamine (c), uric acid (d), glucose (e), Mglycin (f), citric acid (g), acetic acid (h), $MgSO_4$ solutions (j) and NaCl solutions (j)). As seen in Fig. S10, nine tested substances do not interfere the result of testing H_2O_2 significantly. This result might be attributed to the intrinsic selectivity of Hb for its substances.

3.7. Stability and reproducibility of the biosensor

The stability of the Nafion/Hb/H-TiO_2-rGOMS/GCE is investigated through two methods. Firstly, 100 continuous cyclic scans on Nafion/Hb/H-TiO_2-rGOMS/GCE are repeated in the potential range from −0.7 V to 0.1 V at a scan rate of 0.1 V s^{-1} (Fig. 6A). There is almost no decrease of the voltammetric response and 96.3% of the initial current response was retained. Hence, the prepared Nafion/Hb/H-TiO_2-rGOMS/GCE possesses excellent cycle stability. Secondly, the long-term stability which is an important evaluation index for estimating the performance of biosensor is studied by examining its current response during various storage periods. When not in use, the fabricated biosensor is stored at 4 °C. The biosensor retained about 97.3% of its initial response to H_2O_2 after 30 days and 95.4% after 60 days, demonstrating good long-term stability (Fig. 6B). Additionally, compared with that of Nafion/Hb/H-TiO_2-rGOMS/GCE, the stability of Nafion/Hb/TiO_2-rGO/GCE and Nafion/Hb/TiO_2@rGOMS/GCE are relatively worse (Fig. S11). The good stability is probably contributed to special hollow structure and excellent biocompatibility of prepared H-TiO_2-rGO MS which can provide a favorable microenvironment for Hb to retain its bioactivity.

The reproducibility of the biosensor is investigated by determining 4 μM H_2O_2 in PBS (pH 7.0). The relative standard deviation (RSD) is 2.4% respectively for 5 successive measurements. Five biosensors prepared under the same conditions independently give a RSD of 2.7% for the determination of 4 μM H_2O_2 in PBS (pH 7.0), indicating an acceptable electrode-to-electrode reproducibility.

3.8. Analysis of real samples

In order to evaluate the analytical utility of the electrode in practice, the Nafion/Hb/H-TiO_2-rGOMS/GCE is applied for determination of real contact lens care solution. Before experiments, the real samples are diluted 5000 times with doubly distilled water and without any other pretreatment. Recovery tests and $KMnO_4$ titration method were used to examine the reliability and accuracy of this method. The H_2O_2 content of different samples

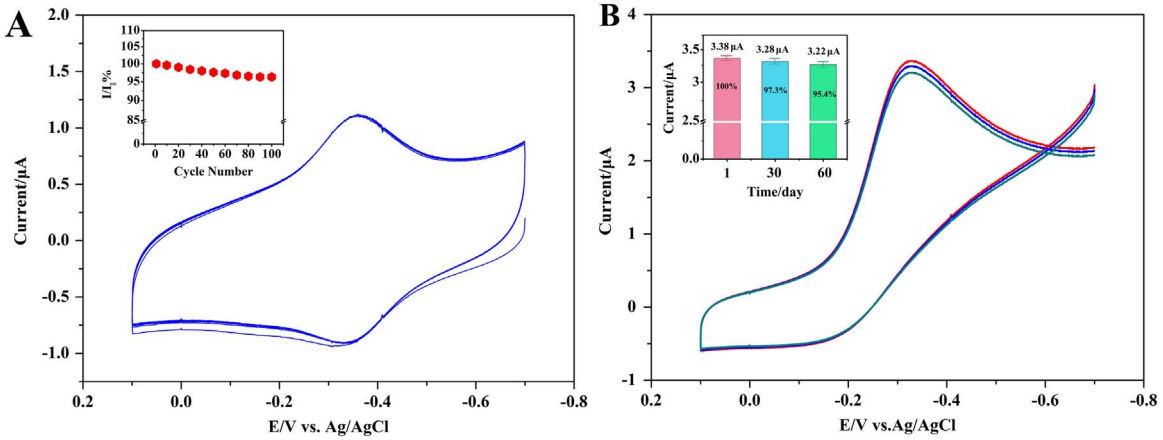

Fig. 6. (A) Cyclic voltammograms of Nafion/Hb/H-TiO_2-rGOMS/GCE in PBS (pH 7.0) with 100 continuous cyclic scans. Scan rate: 100 mV s^{-1}. Inset: the relationship between I/I_0 and the cycle number. I and I_0 correspond to the cathodic peak current on any day and the first day after the preparation. (B) Cyclic voltammograms of Nafion/Hb/H-TiO_2-rGOMS/GCE in 0.1 M pH 7.0 PBS containing 100 μM H_2O_2 on the first day (a), 30th day (b) and 60th day (c) after the preparation. Scan rate: 100 mV s^{-1}. Inset: the relationship between the cathodic peak current and the storage time.

and recoveries of added analyte are evaluated, and the results confirm that determining the H_2O_2 concentration in real samples by using the proposed method is reliable (Table S3).

4. Conclusion

Hollow TiO_2-rGO microspheres have been synthesized through a simple synthetic route, and subsequently used to fabricate a mediator-free biosensor for the detection of H_2O_2. The special hollow structure of microspheres can immobilize more Hb with biological activity, and the graphene can simply entrap the substrate. Hence, there is an increased chance of effective collisions between substrate and redox protein leading to improved performance of this sensor. More importantly, numerous TiO_2 nanoparticles with excellent biocompatibility on the microsphere may provide a protective microenvironment for Hb to retain its bioactivity and stability for long time. Due to the reasons above, the prepared biosensors display a low detection limit of 10 nM, a wide linear range of 0.1–360 μM for H_2O_2, especially an excellent long-term stability. This study indicates that hollow TiO_2-rGO microspheres can be used as biocompatible matrix for the immobilization of enzyme and the construction of direct electrochemical biosensor.

Acknowledgments

This work was financially supported by the National Science Foundation of China (51272147), the Natural Science Foundation of Shaanxi Province (2015JM5208) and the Graduate Innovation Fund of Shaanxi University of Science and Technology.

Appendix A. Supporting information

Supplementary data associated with this article can be found in the online version at http://dx.doi.org/10.1016/j.bios.2016.08.089.

References

Akhavan, O., Ghaderi, E., 2009. J. Phys. Chem. C 113 (47), 20214–20220.
Allen Mattew, J., Tung Vincent, C., Kaner Richard, B., 2010. Chem. Rev. 110 (1), 132–145.
Bai, H., Xu, Y., Zhao, L., Li, C., Shi, G., 2009. Chem. Commun. (13), 1667–1669.
Cao, S., Zhang, L., Chai, Y., Yuan, R., 2013. Biosens. Bioelectron. 42, 532–538.
Chen, X., Wang, Q., Wang, L., Gao, F., Wang, W., Hu, Z., 2015. Biosens. Bioelectron. 66, 216–223.
Dong, L., Gari, R.R.S., Li, Z., Craig, M.M., Hou, S., 2010. Carbon 48 (3), 781–787.
Dong, S., Zhang, P., Liu, H., Li, N., Huang, T., 2011a. Biosens. Bioelectron. 26 (10), 4082–4087.
Dong, S., Zhang, P., Liu, H., Li, N., Huang, T., 2011b. Biosens. Bioelectron. 26 (10), 4082–4087.
Fan, Y., Huang, K.-J., Niu, D.-J., Yang, C.-P., Jing, Q.-S., 2011. Electrochim. Acta 56 (12), 4685–4690.
George, S., Lee, H.K., 2009. J. Phys. Chem. B 113 (47), 15445–15454.
Hummers Jr, W.S., Offeman, R.E., 1958. J. Am. Chem. Soc. 80 (6), 1339–1339.
Jang, H.D., Kim, S.K., Chang, H., Roh, K.-M., Choi, J.-W., Huang, J., 2012. Biosens. Bioelectron. 38 (1), 184–188.
Kamin, R.A., Wilson, G.S., 1980. Anal. Chem. 52 (8), 1198–1205.
Kim, J., Grate, J.W., Wang, P., 2006. Chem. Eng. Sci. 61 (3), 1017–1026.
Kovtyukhova, N.I., Ollivier, P.J., Martin, B.R., Mallouk, T.E., Chizhik, S.A., Buzaneva, E. V., Gorchinskiy, A.D., 1999. Chem. Mater. 11 (3), 771–778.
Kudin, K.N., Ozbas, B., Schniepp, H.C., Prud'Homme, R.K., Aksay, I.A., Car, R., 2008. Nano Lett. 8 (1), 36–41.
Laviron, E., 1979. J. Electroanal. Chem. Interface 101 (1), 19–28.
Lee, J.S., You, K.H., Park, C.B., 2012. Adv. Mater. 24 (8), 1084–1088.
Liu, H., Dong, X., Wang, X., Sun, C., Li, J., Zhu, Z., 2013. Chem. Eng. J. 230, 279–285.
Liu, H., Duan, C., Su, X., Dong, X., Shen, W., Zhu, Z., 2014b. Ceram. Int. 40 (7), 9867–9874.
Liu, H., Duan, C., Su, X., Dong, X., Huang, Z., Shen, W., Zhu, Z., 2014a. Sens. Actuators B: Chem 203, 303–310.
Liu, S., Chen, A., 2005. Langmuir 21 (18), 8409–8413.
Liu, X., Pan, L., Zhao, Q., Lv, T., Zhu, G., Chen, T., Lu, T., Sun, Z., Sun, C., 2012. Chem. Eng. J. 183, 238–243.
Lu, X., Zhang, H., Ni, Y., Zhang, Q., Chen, J., 2008. Biosens. Bioelectron. 24 (1), 93–98.
Ma, W., Tian, D., 2010. Bioelectrochemistry 78 (2), 106–112.
Park, S., Ruoff, R.S., 2009. Nat. Nanotechnol. 4 (4), 217–224.
Park, S., Lee, K.-S., Bozoklu, G., Cai, W., Nguyen, S.T., Ruoff, R.S., 2008. ACS Nano 2 (3), 572–578.
Pham, V.H., Cuong, T.V., Hur, S.H., Oh, E., Kim, E.J., Shin, E.W., Chung, J.S., 2011. J. Mater. Chem. 21 (10), 3371–3377.
Shan, C., Yang, H., Han, D., Zhang, Q., Ivaska, A., Niu, L., 2010. Biosens. Bioelectron. 25 (5), 1070–1074.
Sher Shah, M.S.A., Park, A.R., Zhang, K., Park, J.H., Yoo, P.J., 2012. ACS Appl. Mat. Interfaces 4 (8), 3893–3901.
Stankovich, S., Dikin, D.A., Piner, R.D., Kohlhaas, K.A., Kleinhammes, A., Jia, Y., Wu, Y., Nguyen, S.T., Ruoff, R.S., 2007. Carbon 45 (7), 1558–1565.
Sun, A., Zhao, H., Zheng, J., 2012. Talanta 88, 259–264.
Sun, W., Guo, Y., Ju, X., Zhang, Y., Wang, X., Sun, Z., 2013. Biosens. Bioelectron. 42, 207–213.
Sun, W., Dong, L., Deng, Y., Yu, J., Wang, W., Zhu, Q., 2014a. Mater. Sci. Eng. C 39, 86–91.
Sun, W., Dong, L., Deng, Y., Yu, J., Wang, W., Zhu, Q., 2014b. Mater. Sci. Eng. C 39, 86–91.
Wang, F., Yang, C., Duan, M., Tang, Y., Zhu, J., 2015. Biosens. Bioelectron. 74, 1022–1028.
Wang, S.-F., Chen, T., Zhang, Z.-L., Shen, X.-C., Lu, Z.-X., Pang, D.-W., Wong, K.-Y., 2005. Langmuir 21 (20), 9260–9266.
Xiang, Q., Yu, J., Jaroniec, M., 2012. J. Am. Chem. Soc. 134 (15), 6575–6578.
Xie, Q., Zhao, Y., Chen, X., Liu, H., Evans, D.G., Yang, W., 2011. Biomaterials 32 (27), 6588–6594.
Yu, J., Ma, T., Liu, S., 2011. Phys. Chem. Chem. Phys. 13 (8), 3491–3501.
Zhang, H., Lv, X., Li, Y., Wang, Y., Li, J., 2009. ACS Nano 4 (1), 380–386.
Zhang, Y., Tang, Z.-R., Fu, X., Xu, Y.-J., 2010. ACS Nano 4 (12), 7303–7314.
Zhu, Z., Qu, L., Niu, Q., Zeng, Y., Sun, W., Huang, X., 2011. Biosens. Bioelectron. 26 (5), 2119–2124.